nature nanotechnology

ARTICLES

PUBLISHED ONLINE: 20 DECEMBER 2009 | DOI: 10.1038/NNANO.2009.379

Electrostatic focusing of unlabelled DNA into nanoscale pores using a salt gradient

Meni Wanunu[1], Will Morrison[1], Yitzhak Rabin[2], Alexander Y. Grosberg[3] and Amit Meller[1]*

Solid-state nanopores are sensors capable of analysing individual unlabelled DNA molecules in solution. Although the critical information obtained from nanopores (for example, DNA sequence) comes from the signal collected during DNA translocation, the throughput of the method is determined by the rate at which molecules arrive and thread into the pores. Here, we study the process of DNA capture into nanofabricated SiN pores of molecular dimensions. For fixed analyte concentrations we find an increase in capture rate as the DNA length increases from 800 to 8,000 base pairs, a length-independent capture rate for longer molecules, and increasing capture rates when ionic gradients are established across the pore. Furthermore, we show that application of a 20-fold salt gradient allows the detection of picomolar DNA concentrations at high throughput. The salt gradients enhance the electric field, focusing more molecules into the pore, thereby advancing the possibility of analysing unamplified DNA samples using nanopores.

Solid-state nanopores are an emerging class of single-molecule sensors for characterizing individual unlabelled biopolymers[1–7], as well as DNA–protein[8] and DNA–ligand[9] complexes. Their unique potential for obtaining submolecular information from long, unlabelled double-stranded DNA (dsDNA) molecules is of particular interest in native genome analysis and for proposed nanopore-based DNA sequencing approaches[10,11]. Although nanopore sensing involves reading the properties of long dsDNA molecules as they slide linearly through the pore, it is the initial process of threading into the nanopore that determines the throughput of the method. This capture process consists of two steps: arrival of a molecule from the bulk to the pore mouth, and threading of a polymer end into the pore. Studies of single-stranded DNA capture into lipid-embedded α-haemolysin channels indicate that there is a free energy barrier for DNA capture that is associated with threading of the first few bases[12–15]. Such a barrier was not observed for the capture of dsDNA with lengths of 4–6 kbp (ref. 16) and 48 kbp (λ-phage DNA)[2] into large solid-state pores (diameter >5 nm). Despite the sub-5-nm size regime being the most relevant for many nanopore applications[10], DNA capture into pores in this regime has yet to be characterized.

In this paper, we investigate the capture mechanism for the capture of dsDNA into sub-5-nm solid-state nanopores, as well as its scaling with various experimental parameters. We show that capture involves two main steps, as illustrated in Fig. 1. First, as a DNA coil approaches the pore from bulk (i, Fig. 1a) to a distance larger than the coil size, its motion transitions from purely diffusive to biased motion, driven by the electric field outside the pore. This field is maintained by an ion current across the pore, which creates a potential profile $V(r)$ outside the pore mouth that attracts the DNA coil from a distance r, orders of magnitude greater than Debye screening length scales (0.1–1 nm). Subsequently, a DNA coil experiencing this field is 'funnelled' towards the pore mouth (ii, Fig. 1a). In the second step, once the DNA coil is within approximately one coil size (r_g) of the pore, a DNA end threads into the pore, a process that involves crossing a free-energy barrier (iii, Fig. 1a).

We find that the funnelling field can be enhanced by applying salt gradients across the pore, thereby increasing capture from the bulk. Applying a 20-fold salt gradient increases the nanopore sensitivity by a factor of more than 30, allowing the first nanopore-based analysis of miniscule amounts ($<1 \times 10^6$ copies) of long dsDNA molecules under physiological conditions. Incidentally, the same salt gradients that augment the capture rate also increase mean translocation times, presenting two simultaneous advantages in nanopore sensing[10].

Figure 1b presents a schematic of the setup, which consists of a solitary 3.5-nm pore fabricated in a SiN membrane (a high-resolution transmission electron microscopy image is shown in the bottom panel of Fig. 1a)[17]. Both the analyte (*cis*) and the collection (*trans*) chambers are equipped with a miniature Ag/AgCl electrode. Stochastic threading of a dsDNA end followed by complete translocation generates a distinct square-shaped pulse, allowing statistical analyses of dwell times t_D and mean time delays between two successive events δt, used to define the mean capture rates (see Methods).

DNA capture under symmetric salt conditions

For a small cylindrical pore in an insulating membrane separating two electrolyte solutions, application of potential across the membrane produces an electric field profile away from the pore mouth ($r > 0$), which varies as $V(r) = (d^2/8lr)\Delta V$, where r is the distance from the pore mouth, d the pore diameter, l its length and ΔV the voltage applied to the electrodes (shown in Fig. 1, for derivation see Supplementary text SI-1). In the negatively biased chamber, this field creates an attractive, funnel-shaped potential landscape[18] for the negatively charged DNA, resulting in a space-dependent drift velocity of $v(r) = \mu\nabla V(r)$, where μ is the DNA electrophoretic mobility. As predicted theoretically[19] and confirmed experimentally[20], μ in free solution does not depend on DNA length for DNA longer than a few persistence lengths[21]. This is the result of the free-draining property of an electrophoretically driven DNA coil in solution—electroosmotic flow (EOF) of water induced by oppositely charged counterions

[1]Department of Biomedical Engineering and Department of Physics, Boston University, Boston, Massachusetts 02215, USA, [2]Department of Physics, Institute of Nanotechnology and Advanced Materials, Bar-Ilan University, Ramat-Gan 52900, Israel, [3]Department of Physics, New York University, New York, New York 10003, USA. *e-mail: ameller@bu.edu

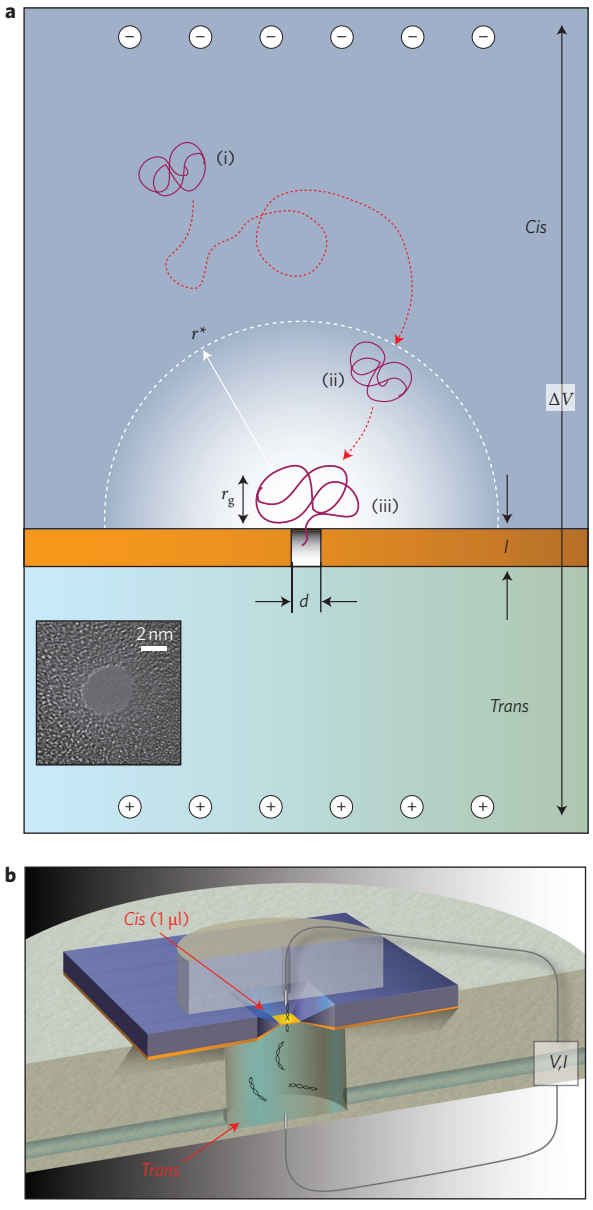

Figure 1 | Biomolecular funnelling into a solid-state nanopore. **a**, The electric potential near small solid-state nanopores attracts negatively charged DNA coils into the nanopore, where individual molecules are detected. Away from the pore (i), the electric field is negligible and DNA motion is purely diffusive, but at distances smaller than r^*, the potential $V(r)$ (where r is the radial distance from the pore mouth into the *cis* chamber, see white arrow) is large enough to funnel DNA in towards the pore mouth (ii). At the pore mouth (iii), an energy barrier describes the final process of threading a DNA end into the pore. Inset: bright-field TEM image of a 3.5-nm solid-state pore fabricated in a 25-nm-thick, low-stress SiN membrane. **b**, Schematic of the solid-state nanopore setup, featuring a microlitre-volume analyte *cis* chamber.

counteracts the long-range hydrodynamic interactions between DNA segments[19].

Although for $r \gg d$ ($d \approx 5$ nm), $V(r) \ll \Delta V$, the effect of $V(r)$ on DNA capture is significant even at large distances from the pore, because it acts on a highly charged macromolecule. Previous studies have shown that a characteristic length scale exists such that DNA motion crosses over from almost purely diffusive at distances $r > r^*$, to drift-dominated motion when $r < r^*$ (refs 2,16,22). We define r^* here by setting $V(r^*) = D/\mu$, where D is the DNA diffusion coefficient,

$$r^* = \frac{d^2\mu}{8lD}\Delta V \quad (1)$$

When the capture rate is limited by the time required for the polymer to arrive at the pore, and not by the final threading process, this can be described by Smoluchowski theory for absorption by a hemisphere of radius r^*. The diffusion-limited current is $J_{\mathrm{diff}} = R_{\mathrm{diff}}\, c$, where c is the bulk DNA concentration and the diffusion-limited capture rate R_{diff} is given by

$$R_{\mathrm{diff}} = 2\pi D r^* = \frac{\pi d^2 \mu}{4l}\Delta V \quad (2)$$

Thus, capture should be DNA length independent in this diffusion-limited regime. Although this result may seem counterintuitive (the free diffusion for larger DNA is slower), the effective capture radius r^* grows with D^{-1}, cancelling out the size dependence.

To test the prediction of equation (2), we measured the capture rate of dsDNA molecules as a function of their length in the range 400–48,502 bp. Figure 2a presents a semi-logarithmic plot of the specific capture rate (events $s^{-1}\,nM^{-1}$) as a function of DNA length. The salient features are fast growth of the capture rate with increasing DNA length from ~1 kbp to ~8 kbp, and a constant capture rate for molecules longer than ~8 kbp. The observed length independence indicates that, for long DNA, capture is limited by driven diffusion to the pore, as equation (2) suggests. In contrast, for DNA shorter than ~8 kbp, diffusion to the pore is not the rate-limiting step for DNA capture.

Recall that DNA capture requires threading one of the polymer ends into the pore (step iii in Fig. 1a). This confinement of the DNA end, as well as possible unfavourable interactions of the highly charged DNA with the pore itself, can create a free energy barrier to capture. This barrier was experimentally observed for DNA transport through the 1.5-nm protein pore α-haemolysin by an exponential dependence of the capture rate on voltage[12,13], and also explained theoretically[15]. In contrast, recent experiments[2,16] and theoretical[22,23] studies of dsDNA transport through large solid-state pores indicate a barrier-free capture process, as indicated by the linear dependence of the capture rate on voltage. We measured the capture rate as a function of voltage and DNA length to explore the free energy landscape of capture into small (<5 nm) solid-state nanopores. Figure 2b displays the specific capture rate into a 4-nm pore as a function of applied voltage ΔV for (i) 400 bp, (ii) 3,500 bp and (iii) 48,502 bp DNA. The capture rates of the short (400 bp) and medium (3,500 bp) DNA lengths display an exponential increase with the applied voltage, yielding slopes of $9.6 \pm 0.4\ V^{-1}$ and $7.1 \pm 0.5\ V^{-1}$, respectively (black lines i and ii in the semi-logarithmic plot in Fig. 2b). In contrast, the capture rates of the longest DNA fragment (iii), which is in the length-independent regime, shows a linear dependence on ΔV (see inset).

When DNA capture is governed by an energy barrier, its rate, according to classical Kramers theory, can be written in the form $J = Rc = \omega \exp[(q\Delta V - U)/k_B T]$, where U is the height of the threading barrier without any voltage applied and q is the effective charge of a DNA end segment, which is independent of DNA length. The pre-factor ω in the expression is usually interpreted as the threading attempt rate. To understand the steep length dependence in the barrier regime, we have to evaluate the influence of the local potential $V(r)$ and DNA length on ω. In this step, the DNA coil is placed at the pore mouth at an average distance approximated by its radius of gyration, r_g. We find that the funnel-shaped potential $V(r)$ near the pore leads to two capture enhancement mechanisms, evaluated in Supplementary text SI-1.

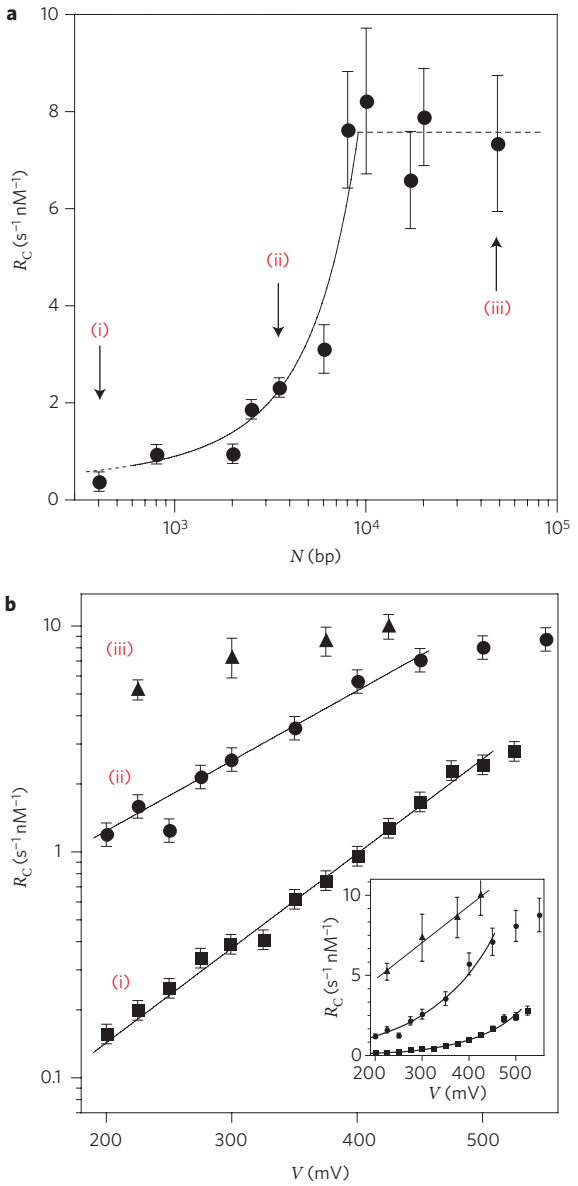

Figure 2 | Dependence of the specific capture rate R_C on DNA length and voltage under symmetric salt conditions. a, Dependence of R_C on DNA length ($\Delta V = 300$ mV). The solid line is the best fit to $A \exp[C(N/4N_p)^{1/2}]$, with $A = 0.31 \pm 0.04$ (nM s)$^{-1}$ and $C = 0.81 \pm 0.15$ for $800 < N < 8{,}000$ bp and N_p represents the number of base pairs in a dsDNA persistence length. For $N > 8{,}000$ bp, we observe a transition to an N-independent regime (dashed line). **b**, Dependence of R_C on the applied voltage for: (i) 400 bp, (ii) 3,500 bp and (iii) 48,502 bp DNA. The capture rates of the short (400 bp) and medium (3,500 bp) DNA lengths display an exponential increase with applied voltage (lines), but the capture rate of the 48,502 bp DNA fragment shows a linear dependence on ΔV (see inset). Error bars in **a**,**b** are based on the reduced chi-square values from the fits (see Methods).

The first is an enhancement in exponential attempt rate, resulting from the fact that the potential well $V(r)$ traps the DNA a distance r_g from the pore mouth, where threading is repeatedly attempted. Because of the energy barrier, DNA molecules are delivered to the pore mouth many times before a successful translocation occurs. Therefore, although the probability of finding a DNA coil within a distance r_g from the pore mouth is cr_g^3 in the absence of $V(r)$, the presence of $V(r)$ enhances this probability by the exponential factor $\exp(Ne\alpha/k_BT)$. In this case, the effective charge of the DNA is proportional to its length N. This is different from the N-independent electrophoretic mobility of DNA in bulk (μ above), because when the DNA coil is pressed against the membrane, hydrodynamic (electroosmotic) flow through it is suppressed (the pore diameter is much smaller than the DNA coil). In the second mechanism, when the DNA coil is placed at the pore mouth, the probability of successful end threading into the pore is determined by the internal dynamics of the coil. Although the coil relaxation time is estimated by its Zimm time (τ_{Zimm}), its dynamics is affected by the potential $V(r)$, which attracts the chain ends towards the pore, providing further rate enhancement. Together, these two effects result in an increased capture rate, R_{bar},

$$R_{bar} = \frac{r_g^3}{\tau} \exp\left[\frac{q\Delta V - U}{k_B T} + \frac{e\Delta V}{k_B T}\frac{\alpha d^2}{al}\left(\frac{N}{4N_p}\right)^{1/2}\right] \qquad (3)$$

where τ is proportional to $\tau_{Zimm}(kT/e\Delta V)(8la/d^2)$, $N_p \approx 150$ is the number of base pairs in a dsDNA persistence length, a is the length per base pair of dsDNA, and α is a constant related to the fact that not all phosphates on the DNA are ionized due to Onsager–Manning condensation. We consider equation (3) to be valid only for sufficiently long DNA, that is, $N > 4N_p$. Because $\tau_{Zimm} \propto r_g^3$, the only dependence on DNA length in equation (3) appears in the second term of the exponent, namely $R_{bar} \approx \exp[C(N/4N_p)^{1/2}]$.

When $R_{diff} > R_{bar}$, the capture rate is limited by the barrier crossing given by equation (3). This can only be realized when the threading barrier is sufficiently large (that is, for narrow enough nanopores). In this barrier-dominated regime, R_{bar} grows with DNA length. When R_{bar} becomes sufficiently large, the rate-limiting step becomes diffusion to the pore. Capture rate in this regime is proportional to R_{diff}, and independent of N (equation (2)). The overall capture rate is thus expected to exhibit a transition from a rapidly growing function with N ($\sim\exp[C(N/4N_p)^{1/2}]$) to a length-independent plateau for long enough DNA molecules.

In Fig. 2a, this prediction is overlaid with our experimental data. For molecules in the range ~800–8,000 bp, the capture rate per nM of DNA molecules can be fitted well by equation (3) (see solid line), which agrees with the hypothesis that in this range the process is dominated by a free energy barrier. In the range 8,000–48,000 bp, we observe the length-independent, diffusion-dominated regime. The fit also provides the value of the dimensionless constant $C = (e\Delta V/k_BT)(\alpha d^2/al) = 0.81 \pm 0.15$. The rapidly growing capture rate with N in sub-5-nm pores represents a distinct example of capture selectivity towards longer DNA molecules, which is surprising, considering the length-independent DNA mobility in free-flow electrophoresis. When barrier crossing is the rate-limiting step, longer DNA molecules are more efficiently threaded than short ones, as their higher charge is advantageous for funnelling into the pore mouth.

Increasing the capture rate with ion gradients

The strong impact of $V(r)$ on the capture rate suggests that manipulation of the voltage profile outside the pore is of potential utility for increasing throughput. Although increasing the applied voltage ΔV also increases $V(r)$, translocation times become exponentially shorter[7], decreasing the method's resolution. In contrast, we find that an ion gradient across the pore can be used to significantly enhance the magnitude of $V(r)$ in the *cis* chamber, greatly enhancing the capture rate without reducing the translocation times. This finding is illustrated in Fig. 3. Using the same pore, we measured R_C at 1 M/1 M *trans*/*cis* KCl concentrations, replaced the buffers with 1 M/0.2 M, and then 0.2 M/1 M, while maintaining a constant concentration of 3.8 nM 400 bp DNA in the *cis* chamber (Fig. 3a, top to bottom). Continuous data streams were collected for each gradient, and representative two-second snapshots are shown. Strikingly, when the *cis* concentration was lowered

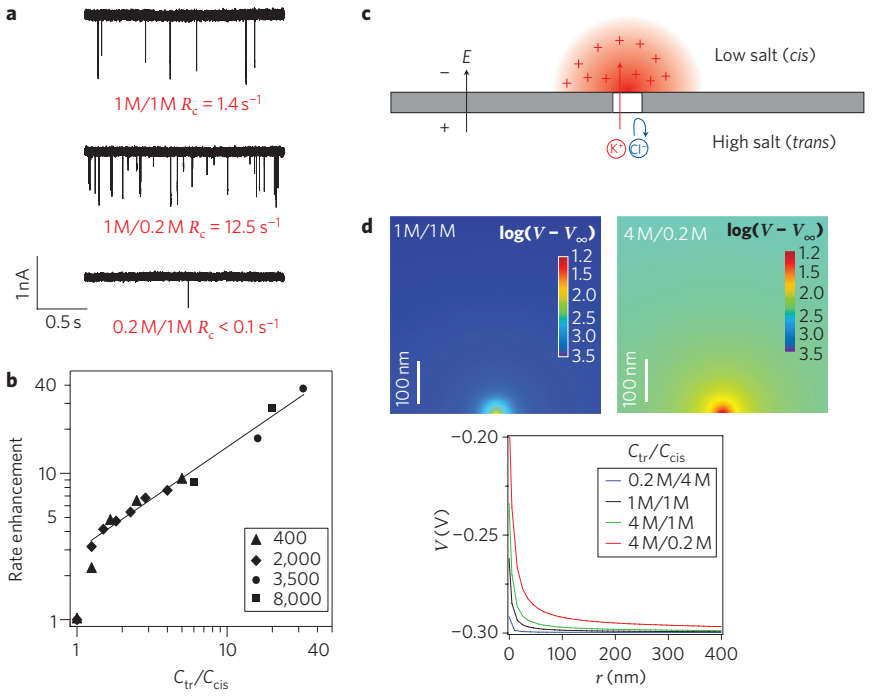

Figure 3 | Capture rate enhancement using a salt gradient across the nanopore. a, Continuous traces measured using a 3.5-nm pore with 3.8 nM 400 bp DNA for different indicated (C_{tr}/C_{cis}) KCl concentrations. The average capture rate is specified in each case. **b**, DNA capture rate enhancement for four different DNA lengths as a function of C_{tr}/C_{cis}, relative to $C_{tr}/C_{cis} = 1$. **c**, Schematic showing the creation of an asymmetric salt gradient across the pore, where $C_{tr}/C_{cis} > 1$, results in selective pumping of cations (K^+) from *trans* to *cis*, creating a local positive concentration of ions near the pore (reddish area), which results in rate enhancement. **d**, Electric potential maps evaluated numerically in the *cis* side of the pore, for both symmetric (top left) and asymmetric (bottom left) KCl concentrations. The pore mouth is positioned at the bottom centre of each image. The potential range outside the pore increases with salt asymmetry. Right panel: axial dependence of the potential as a function of distance from the pore mouth *r*, shown for four different salt gradients, as indicated.

from 1 M to 0.2 M, the capture rate increased ninefold from ~0.4 to ~3.7 $s^{-1}nM^{-1}$. Reversal of the conditions (to 0.2 M/1 M) effectively suppressed DNA capture. These results were completely reversible, in that changing back to 1 M/1 M yielded the same capture rate as previously obtained with those concentrations.

We measured the capture rate over a range of experimental conditions. Figure 3b shows the enhancement in R_C for several DNA lengths (400 bp, 2,000 bp, 3,500 bp and 8,000 bp), and over a large range of asymmetries (C_{tr}/C_{cis} from 1 to ~32). Clearly, above a threshold value of approximately $C_{tr}/C_{cis} \approx 1.5$ a linear, length-independent increase in the capture rate is observed. In addition to the rate enhancement, our asymmetric salt conditions allow experiments under physiological conditions (down to 125 mM KCl) while preserving the signal-to-noise ratio (Supplementary text SI-6).

These experimental observations can be explained by the dependence of $V(r)$ on the ionic environment in the vicinity of the pore. Under symmetric ionic strengths, the electric field across the pore equally drives K^+ ions from *trans* to *cis* and Cl^- ions from *cis* to *trans*, creating a symmetric steady-state ion flux (neglecting electroosmosis; Supplementary text SI-6). In contrast, under asymmetric salt conditions, the applied voltage may result in cation selectivity. Consider the case shown schematically in Fig. 3c, where the salt concentration in the *cis* chamber is much lower than in the *trans*; under typical fields applied to nanopores (~1×10^5 V cm^{-1}, positive voltage to the *trans* chamber), diffusion of Cl^- ions from the *trans* to *cis* chamber down the concentration gradient is hindered by the applied potential (a transported Cl^- ion must overcome an electric potential energy of ~0.3 eV, corresponding to ~$12k_BT$). In contrast, K^+ ions are pumped from *trans* to *cis*, moving in the direction of both the chemical and electrical potential gradients. As positive ions are continuously pumped into the *cis* chamber, the pore vicinity is effectively polarized and the magnitude of $V(r)$ increases. This effect enhances the capture rate in both the diffusion-limited and barrier-limited regimes.

Under asymmetric salt conditions, our theory (Supplementary text SI-1) predicts that, to a first approximation, $V(r)$ is proportional to the ratio of bulk ionic concentrations in the *cis* and *trans* chambers: $V(r) = V_{sym}(r)C_{tr}/C_{cis}$, where $V_{sym}(r)$ is the potential under symmetric conditions. Accordingly, the value of r^* is also modified to $r^* = r^*_{sym}C_{tr}/C_{cis}$. The rationale behind this is that the voltage drop in the solution of lower conductance is higher and, therefore, a high/low *trans*/*cis* salt gradient will yield an asymmetric potential profile, with more of the voltage dropping in the *cis* chamber than the *trans* chamber. Finite-element COMSOL simulations (Fig. 3d and Supplementary text SI-2) confirm that salt-dependent charge imbalance at the pore results in a significant increase in the protrusion of the potential into the *cis* chamber for large C_{tr}/C_{cis}. Notably, for $C_{tr}/C_{cis} = 20$ (4 M/0.2 M KCl), $V(r)$ remains considerable hundreds of nanometres away from the pore (Fig. 3d, red curve).

One may ask whether the funnelling effect near the pore also induces faster DNA sliding, which would be problematic for current nanopore sensing methods[10]. We find, however, that the enhanced capture rate with increasing salt gradients is accompanied by longer DNA translocation times (Supplementary text SI-5). This can be explained by a combination of two effects. First, an increased EOF of K^+ counterions along the DNA and pore surface provides a drag force opposing DNA motion in the pore, as shown by molecular dynamics simulations[24] and direct single-molecule force measurements[25]. The weakly negatively charged nanopore surface also contributes somewhat to the EOF of the K^+ ions from *trans* to *cis*, as supported by the pH dependence on conductance of uncoated and amine-modified SiN pores[26], as well as by capture

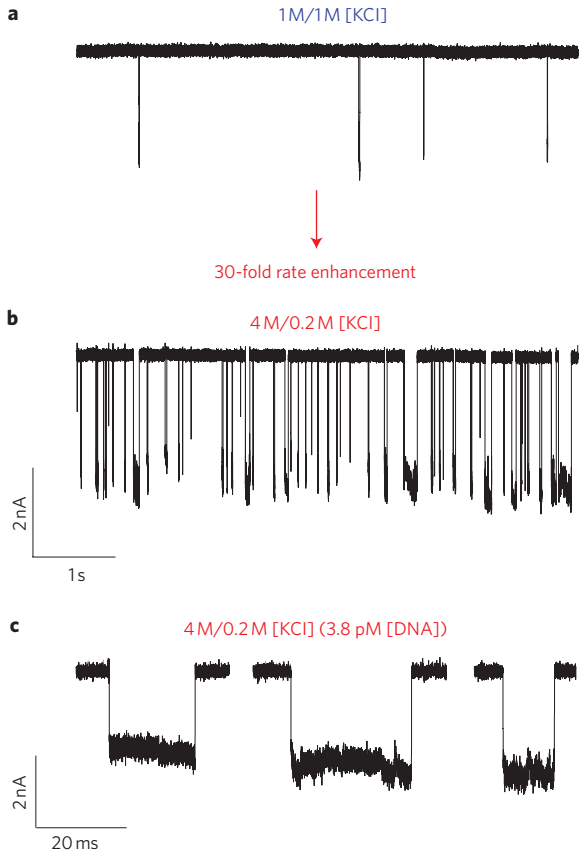

Figure 4 | Picomolar detection of unlabelled DNA under asymmetric salt concentrations. a, Continuous current trace under symmetric (1 M/1 M) salt concentrations (38 pM solution of 8,000 bp fragment) showing an average rate of 0.4 s^{-1}. **b**, Under asymmetric salt concentrations (0.2 M/4 M) a 30-fold increase in capture rate is observed compared with **a. c**, Reduction of the DNA concentration tenfold to ~3.8 pM (only ~4 attomole in the 1 μl *cis* chamber) resulted in a high capture rate (~1 s^{-1}), with a markedly longer translocation time when compared with the symmetric salt conditions and good signal/background ratio.

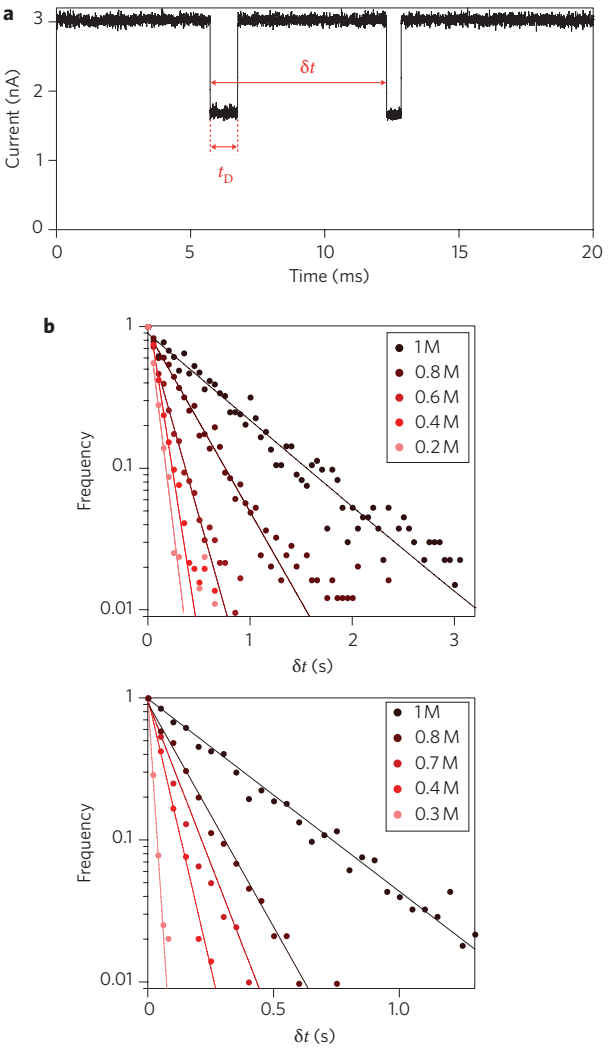

Figure 5 | Measurement of the capture rate from single-molecule ion-current blockades. a, A typical ion-current trace flowing through a 3.5 nm pore in the presence of 8,000 bp DNA (1 M KCl, 300 mV, 21 °C). We define here the time delay between successive events δ*t* and the DNA transport time, or dwell time t_D. **b**, Representative δ*t* distributions measured for 400 bp DNA (top panel) and 2,000 bp DNA (bottom panel), measured at the indicated *cis* chamber KCl concentrations and 1 M concentration at the *trans* chamber.

measurements of a neutral polymer (Supplementary text SI-7). Second, the actual voltage drop inside the pore is a function of the salt gradient conditions, and a higher voltage drop outside the pore diminishes the electrophoretic field inside the pore.

Tuning up the capture rate using salt gradients facilitates the detection of trace quantities of DNA. We miniaturized the *cis* chamber to a volume of 1 μl (see Fig. 1b) and recorded current traces of a 38 pM solution of 8,000 bp DNA (~1×10^7 copies), switching from symmetric (1 M/1 M) to highly asymmetric (4 M/0.2 M) salt conditions (see Fig. 4a and b, respectively), resulting in a 30-fold enhancement in capture rate. The large capture rate allowed the concentrated DNA solution to be exchanged with a 3.8 pM solution (Fig. 4c), while still preserving a steady capture rate of ~1 s^{-1}. Collection of >1,000 events over 15 min, followed by characterization of the translocation dynamics, revealed a mean translocation time of ~20 ms, a factor of three longer than for the 1 M/1 M conditions. In total, the 1 μl chamber contained under 4 attomoles, or under 1×10^6 copies of DNA.

We have shown here that salt gradients provide a practical method to controllably tune and enhance the capture rate of DNA molecules into sub-5-nm pores. Moreover, we have observed capture selectivity towards longer DNA molecules, a direct consequence of the interaction of the potential near the pore with the highly charged polymer. DNA detection experiments using nanopores typically use analyte concentrations in the nanomolar to micromolar range for obtaining average capture rates of ~1 event per second, corresponding to 1×10^{10} to 1×10^{13} copies for a 10-μl *cis* chamber. Here, we presented results that allow us to decrease the DNA concentration to the picomolar level, enabling characterization of an attomole-sized sample of DNA in a simple configuration. Our model has yielded a number of clear predictions, such as a growing $\sim\exp[C(N/4N_p)^{1/2}]$ dependence of capture rate on DNA length in the energy barrier dominated regime, and an *N*-independent rate for the diffusion-limited regime. This model also explains the universal scaling of the capture enhancement with the salt asymmetry. Finally, the longer DNA translocation times in the presence of salt gradients provide a means to increase the resolution of the method, while simultaneously enhancing its throughput. These findings facilitate future nanopore studies of biomolecular complexes under physiological conditions and studies of native (unamplified) genomes. These findings may also be of use for the separation of charged polymers and biopolymers using

nanoporous membranes, as the physics should also be applicable to nanopore arrays.

Methods

Nanopores were fabricated in 25-nm-thick, low-stress SiN windows ($25 \times 25\ \mu m^2$) supported by a silicon chip (Protochips) using a focused electron beam, as previously described[17]. Nanopore chips were cleaned in piranha solution and assembled on a custom-designed cell under a controlled atmosphere (see ref. 27 for details). After the addition of degassed and filtered KCl electrolyte (all electrolytes were adjusted to pH 8.5 using 10 mM Tris-HCl), the nanopore cell was placed in a custom-designed chamber featuring thermoelectric regulation within $\pm 0.1\ ^{\circ}C$, rapid thermal equilibration (<5 min), and an effective electromagnetic shield. Homemade Ag/AgCl electrodes were immersed in each chamber of the cell and connected to an Axon 200B headstage. All measurements were taken inside a dark Faraday cage. When the electrodes were dipped directly in two chambers containing a salt gradient, the voltage offset values were found to be purely Nernstian; that is, $V_{off} = -.058 \times \log([Cl^-]_{cis}/[Cl^-]_{trans})$ V. Therefore, before each experiment the voltage across the electrodes was nullified, either by the voltage compensation knob on the Axopatch or by the use of an agarose bridge. DNA solutions were prepared from stock solutions in the respective salt buffers, added to the *cis* chamber, and left for ~3 min for equilibration before measurements were made. Linear, blunt-ended dsDNA fragments were purchased from Fermentas (NoLimits®) and further verified to be pure by agarose gel electrophoresis. λ-Phage DNA was purchased from New England Biolabs, and was diluted and heated to 70 °C for 10 min before each experiment to destabilize concatamers.

DNA translocation data were acquired using custom LabVIEW software, which collects either continuous recording or real-time detection of current pulses. The analogue signal from the amplifier was low-pass filtered at 75 kHz and fed to a DAQ card, which sampled the data at 250 kHz/16 bit. Data were exported to IGOR Pro software, with which curve fits were performed (in all cases, R^2 values for the fits were greater than 0.97). The DNA sample was then characterized by statistical analysis of the square pulse widths (dwell times, t_D) of thousands of molecules, as shown in Fig. 5a. Capture rates were calculated for each experiment from the mean time delay between two successive events, δt. Figure 5b displays semi-logarithmic time-delay distributions for 400 bp (top) and 2,000 bp (bottom) DNA, in which the KCl concentration in the *trans* chamber was kept at 1 M, and the *cis* chamber KCl concentrations were decreased to the indicated concentrations. Typically, $>1 \times 10^3$ events were recorded for each experiment. In all cases, the time-delay distributions fit mono-exponentials $P_C(t) = A \exp(-t/\tau)$ (Fig. 5), as expected from a stochastic capture process with non-interacting molecules (valid in our regime of concentrations). The average capture rates are then reported as τ^{-1} from the fits. For both symmetric and asymmetric salt gradients, we have verified that the capture rate scales linearly with DNA bulk concentration c, as shown in Supplementary text SI-3. Finite-element simulations were performed using COMSOL Multiphysics software. To simulate our experimental situation, we used the full Nernst–Planck equations for the ionic concentrations and Poisson's equation for the electrostatic potential. The system was analysed in the steady state by placing each chamber in contact with a bath maintained at specified concentrations (this is a reasonable approximation, considering the large size of the *cis* and *trans* chambers in comparison with the integrated ionic current through the pore in a typical experiment). The nanopore was hourglass-shaped in all COMSOL simulations, to match the pore geometry measured by TEM tomography[17].

Received 10 August 2009; accepted 12 November 2009; published online 20 December 2009

References

1. Li, J., Gershow, M., Stein, D., Brandin, E. & Golovchenko, J. A. DNA molecules and configurations in a solid-state nanopore microscope. *Nature Mater.* **2,** 611–615 (2003).
2. Chen, P. *et al.* Probing single DNA molecule transport using fabricated nanopores. *Nano Lett.* **4,** 2293–2298 (2004).
3. Storm, A. J. *et al.* Fast DNA translocation through a solid-state nanopore. *Nano Lett.* **5,** 1193–1197 (2005).
4. Smeets, R. M. *et al.* Salt dependence of ion transport and DNA translocation through solid-state nanopores. *Nano Lett.* **6,** 89–95 (2006).
5. Heng, J. B. *et al.* The electromechanics of DNA in a synthetic nanopore. *Biophys. J.* **90,** 1098–1106 (2006).
6. McNally, B., Wanunu, M. & Meller, A. Electro-mechanical unzipping of individual DNA molecules using synthetic sub-2-nm pores. *Nano Lett.* **8,** 3418–3422 (2008).
7. Wanunu, M., Sutin, J., McNally, B., Chow, A. & Meller, A. DNA translocation governed by interactions with solid state nanopores. *Biophys. J.* **95,** 4716–4725 (2008).
8. Smeets, R. M. M., Kowalczyk, S. W., Hall, A. R., Dekker, N. H. & Dekker, C. Translocation of recA-coated double-stranded DNA through solid-state nanopores. *Nano Lett.* **9,** 3089–3095 (2009).
9. Wanunu, M., Sutin, J. & Meller, A. DNA profiling using solid-state nanopores: detection of DNA-binding molecules. *Nano Lett.* **9,** 3498–3502 (2009).
10. Branton, D. *et al.* The potential and challenges of nanopore sequencing. *Nature Biotechnol.* **26,** 1146–1153 (2008).
11. Clarke, J. *et al.* Continuous base identification for single-molecule nanopore DNA sequencing. *Nature Nanotech.* **4,** 265–270 (2009).
12. Henrickson, S. E., Misakian, M., Robertson, B. & Kasianowicz, J. J. Driven DNA transport into an asymmetric nanometer scale pore. *Phys. Rev. Lett.* **85,** 3057–3060 (2000).
13. Meller, A. & Branton, D. Single molecule measurements of DNA transport through a nanopore. *Electrophoresis* **23,** 2583–2591 (2002).
14. Meller, A. Dynamics of polynucleotide transport through nanometre-scale pores. *J. Phys. Condens. Matter* **15,** R581–R607 (2003).
15. Zhang, J. & Shklovskii, B. I. Effective charge and free energy of DNA inside an ion channel. *Phys. Rev. E* **75,** 021906 (2007).
16. Gershow, M. & Golovchenko, J. A. Recapturing and trapping single molecules with a solid-state nanopore. *Nature Nanotech.* **2,** 775–779 (2007).
17. Kim, M. J., Wanunu, M., Bell, D. C. & Meller, A. Rapid fabrication of uniformly sized nanopores and nanopore arrays for parallel DNA analysis. *Adv. Mater.* **18,** 3149–3153 (2006).
18. Schmidt, C., Mayer, M. & Vogel, H. A chip-based biosensor for the functional analysis of single ion channels. *Angew Chem. Int. Ed.* **39,** 3137–3140 (2000).
19. Long, D., Viovy, J.-L. & Ajdari, A. Simultaneous action of electric fields and nonelectric forces on a polyelectrolyte: motion and deformation. *Phys. Rev. Lett.* **76,** 3858–3861 (1996).
20. Nkodo, A. E. *et al.* Diffusion coefficient of DNA molecules during free solution electrophoresis. *Electrophoresis* **22,** 2424–2432 (2001).
21. Olivera, B. M., Baine, P. & Davidson, N. Electrophoresis of the nucleic acids. *Biopolymers* **2,** 245–257 (1964).
22. Wong, C. T. A. & Muthukumar, M. Polymer capture by electro-osmotic flow of oppositely charged nanopores. *J. Chem. Phys.* **126,** 164903 (2007).
23. Chou, T. Enhancement of charged macromolecule capture by nanopores in a salt gradient. *J. Chem. Phys.* **131,** 034703 (2009).
24. Luan, B. & Aksimentiev, A. Electro-osmotic screening of the DNA charge in a nanopore. *Phys. Rev. E* **78,** 021912 (2008).
25. Dorp, S. V., Keyser, U. F., Dekker, N. H., Dekker, C. & Lemay, S. G. Origin of the electrophoretic force on DNA in solid-state nanopores. *Nature Phys.* **5,** 347–351 (2009).
26. Wanunu, M. & Meller, A. Chemically-modified solid-state nanopores. *Nano Lett.* **7,** 1580–1585 (2007).
27. Wanunu, M. & Meller, A. *Single Molecule Analysis of Nucleic Acids and DNA–Protein Interactions using Nanopores* (Cold Spring Harbor Press, 2008).

Acknowledgements

The authors would like to thank B. McNally for help in data acquisition, and support from Harvard's Center for Nanoscale Systems (CNS). We are grateful for stimulating and fruitful discussions with M. Frank-Kamenetskii, A. Kolomeisky, O. Krichevsky, G. Lakatos, D.R. Nelson, A. Parsegian and B. Shklovskii. A.M. acknowledges support from National Institutes of Health award HG-004128 and National Science Foundation award PHY-0646637. Y.R. and A.G. acknowledge support by the US–Israel Binational Science Foundation. Y.R. acknowledges a grant from the Israeli Science Foundation and the hospitality of the NYU Department of Physics.

Author contributions

A.M. and M.W. designed the experiments. M.W. performed all experiments and analysed the data. W.M. performed finite element simulations. Y.R. and A.G. developed the theoretical model. M.W., W.M., Y.R., A.G. and A.M. co-wrote the paper. All authors discussed the results and commented on the manuscript.

Additional information

The authors declare no competing financial interests. Supplementary information accompanies this paper at www.nature.com/naturenanotechnology. Reprints and permission information is available online at http://npg.nature.com/reprintsandpermissions/. Correspondence and requests for materials should be addressed to A.M.